

Comprehensive Molecular-level Understanding of MgO Hydration through Computational Chemistry

Taichi Inagaki^{*,†} and Miho Hatanaka^{†,‡}

Department of Chemistry, Faculty of Science and Technology, Keio University, 3-14-1 Hiyoshi, Kanagawa 223-8522, Japan, and Institute for Molecular Science, Okazaki, Aichi 444-8585, Japan

E-mail: taichi.inagaki@keio.jp

^{*}To whom correspondence should be addressed

[†]Department of Chemistry, Faculty of Science and Technology, Keio University, 3-14-1 Hiyoshi, Kanagawa 223-8522, Japan

[‡]Institute for Molecular Science, Okazaki, Aichi 444-8585, Japan

Abstract

The hydration of magnesium oxide (MgO) to magnesium hydroxide (Mg(OH)_2) is a fundamental solid-surface chemical reaction with significant implications for materials science. Yet its molecular-level mechanism from water adsorption to Mg(OH)_2 nucleation and growth remains elusive due to its complex and multi-step nature. Here, we elucidate the molecular process of MgO hydration based on structures of the MgO /water interface obtained by a combined computational chemistry approach of potential-scaling molecular dynamics simulations and first-principles calculations without any *a priori* assumptions about reaction pathways. The result shows that the Mg^{2+} dissolution follows the dissociative water adsorption. We find that this initial dissolution can proceed exothermically even from the defect-free surface with an average activation barrier of ~ 12 kcal/mol. This exothermicity depends crucially on the stabilization of the resulting surface vacancy, achieved by proton adsorption onto neighboring surface oxygen atoms. Further Mg^{2+} dissolution then occurs in correlation with proton penetration into the solid. Moreover, we find that the Mg(OH)_2 nucleation and growth proceeds according to the dissolution-precipitation mechanism, rather than a solid-state reaction mechanism involving a direct topotactic transformation. In this process, Mg^{2+} ions migrate away from the surface and form amorphous Mg-OH chains as precursors for Mg(OH)_2 nucleation. We also demonstrate that sufficient water facilitates the formation of more ordered crystalline nuclei. This computational study provides a comprehensive molecular-level understanding of MgO hydration, representing a foundational step toward elucidating the mechanisms of this class of complex and multi-step solid-surface chemical reactions.

1 Introduction

Chemical reactions on solid surfaces are fundamental processes and often involve structural transformations of the solid material itself. Such transformative reactions are ubiquitous, ranging from natural phenomena such as metal corrosion and mineral weathering to industrial applications such as heterogeneous catalytic reactions. While these reactions can be understood from a macroscopic perspective as a simple phase change based on thermodynamic chemical equilibrium,^{1–3} at the microscopic level they involve many elementary processes (e.g., chemical bond breaking/forming and atomic migration) in a multi-step and non-equilibrium manner over a wide range of time scales. Due to this complexity, understanding such reactions at the molecular level remains a formidable challenge for both experimental and theoretical/computational approaches. Their detailed elucidation is therefore an important objective in interfacial chemistry.

One such chemical reaction is the hydration of magnesium oxide (MgO) to magnesium hydroxide (Mg(OH)₂), $\text{MgO} + \text{H}_2\text{O} \rightarrow \text{Mg}(\text{OH})_2$. This exothermic transformation of rock-salt MgO into Mg(OH)₂ nanosheets ($\Delta H \sim -81 \text{ kJ/mol}$) involves a simply structured solid and ubiquitous water. Owing to this structural and electronic simplicity, this reaction has been used as a model system to study the interfacial properties of oxide-water systems.⁴ In addition, this hydration reaction is deeply related to various industrial technologies, including heat storage,^{5–7} cement production,^{8–10} and catalysis,^{11,12} and thus also holds practical significance. However, the detailed mechanism at the molecular level remains elusive, hindering efforts to precisely control the reaction's thermodynamics and kinetics for industrial purposes.^{7,13,14}

Early studies of the reaction between MgO surfaces and water have primarily focused on the interfacial structure of water and its molecular dissociation. This hydration reaction starts with the adsorption of water molecules on the surface. The adsorption structure of water molecules at low temperatures has been investigated in detail in previous studies,^{15–24} and the structure has been almost established. In particular, the well-ordered water monolayer structures with *c*(4×2) and *p*(3×2) symmetries have been revealed by theoretical and experimental studies.²⁴ Molecular-level analyses have also shown that water molecules can easily dissociate, even in the monolayer on the

perfect MgO (100) surface, by accepting a strong hydrogen bond (HB) from a neighboring water molecule.²¹ In recent years, a stable adsorption structure under ambient conditions was proposed to be *p*(3×2) symmetry with eight water molecules involving 25% dissociation,²⁵ and the structure was compared with the vibrational sum frequency generation spectroscopy measurements.²⁶ These extensive studies have greatly advanced the understanding of the adsorption and dissociation processes of water molecules.

While the initial dissociative water adsorption under ambient conditions are becoming well-understood, the subsequent elementary processes on the MgO/water interface remain less clear. A crucial next step is widely considered to be the dissolution of Mg²⁺ ions from the surface. Following Ončák and co-workers,²⁷ we use "dissolution" also in the sense that Mg²⁺ ions leave the surface layer and are located above the MgO surface. At the molecular level, theoretical studies found locally stable reconstructed interfaces with Mg²⁺ ions above the surface,^{27–32} which appears relatively consistent with the experimental findings.³³ In particular, these calculations have identified various intermediate states, such as semi-detached Mg²⁺ ions at the low-coordinated edge sites²⁸ or hydrated/hydroxylated contact ion pairs above the surface,³¹ as likely exothermic precursors to dissolution and Mg(OH)₂ formation. These observations suggest that the dissolution of Mg²⁺ ions plays an important role in the early stage of the hydration. However, a significant limitation in these studies is that the dissolution is induced artificially within the theoretical calculations. Therefore, it remains inconclusive whether Mg²⁺ dissolution is the definitive spontaneous process following water adsorption and what the key factors for exothermic dissolution are.

Another important focus for further understanding the hydration is the nucleation and growth mechanism of Mg(OH)₂ crystals, which is still a controversial issue.^{13,17,28,30,32,34–44} One of the notable mechanisms is a direct transformation of the solid structure based on a topotactic relationship between the MgO (111) and Mg(OH)₂ (0001) planes.⁴⁵ In this study, we refer to this as the solid-state reaction mechanism. This mechanism posits that the (0001) planes in Mg(OH)₂ are formed parallel to the (111) planes in MgO. Wogelius *et al.* proposed,³⁴ on the basis of the results of their elastic recoil detection analysis and theoretical calculations, that the hydration proceeds

by the diffusion of bulk Mg^{2+} ions outward and protons (H^+) from water molecules inward in the direction parallel to the MgO (111) planes. The diffusion processes were also expected to be realized together with the creation of a penetrative hydroxylated channel with help from pits,¹⁷ and the channels would result in the interlayer spaces in $Mg(OH)_2$ crystals. This mechanism has also been examined in theoretical studies.^{28,35,46,47} For instance, some studies have mentioned that parts of the reconstructed MgO surface structures closely resemble the $Mg(OH)_2$ structure.^{27,46,47} In particular, Jug and co-workers presented an atomistic process where the MgO surface is dug along the (111) plane by diffusion of Mg^{2+} ions and protons and eventually the (0001) surface of $Mg(OH)_2$ is formed along the MgO (111) plane.³⁰ Recently, Ishida and Ishimura revisited the hydration process proposed by Jug *et al.* using more accurate (density functional theory) calculations.³² In their study, they suggested that the rate-determining step in this mechanism is an extraction of Mg atoms from an inner layer to the aqueous surface layer. It should be noted that these calculations are again based on an artificially determined reaction pathway and therefore are not necessarily examples of the formation of crystal nuclei. In addition, they have not demonstrated the formation of well-ordered $Mg(OH)_2$ nuclei.

An alternative explanation is that nucleation and growth proceeds according to a dissolution-precipitation mechanism. In this process, a hydroxylated MgO surface layer dissolves in water, leading to the aggregation of dissolved species and subsequent nucleation. These nuclei then precipitate due to the low solubility of $Mg(OH)_2$. This dissolution-precipitation mechanism was proposed at an early time,⁴⁸ and the relevant insights are still being provided by experimental studies.^{13,40–44,49–51} For instance, Luong and co-workers demonstrated that a thick water layer on the solid surface is crucial for facilitating the reactions,^{50,51} which indicates that limited water availability delays nucleation. In addition, Bracco and co-workers showed that while a reaction layer forms rapidly on the MgO surface even under relatively dry conditions, it does not continue to grow over time.⁴⁴ They also indicated that the layer on the surface consists of amorphous or poorly crystalline phases rather than crystalline $Mg(OH)_2$.⁴⁴ Their observations imply that the nucleation and growth is favored in an aqueous environment. Overall, recent experimental studies

seems to adopt the dissolution-precipitation mechanism, without examining the possibility of the solid-state reaction mechanism, as a foundational premise for their analysis. An investigation by Chen *et al.* is one of the few theoretical studies^{41,51} to follow the dissolution-precipitation mechanism. Although their calculations focused only on small clusters, they suggested that the self-assembly of extremely small sheet-like Mg(OH)₂ clusters is a possible pathway for the formation of larger Mg(OH)₂ nanoparticles.⁴¹ Thus, while various studies have focused on these different mechanisms, elucidating which mechanism is more plausible through direct comparison remains a pivotal and unresolved question for achieving a molecular-level understanding of MgO hydration.

In this study, we investigate molecular processes in MgO hydration based on computationally obtained MgO/water interfacial structures. We consider an MgO solid surface with the (100) plane initially covered by a water film of two-monolayer thickness. The (100) plane of MgO is known to be the most stable surface in the atmospheric environment. According to previous experimental and theoretical studies,^{27,51,52} a water coverage of two monolayers corresponds to a relatively high humidity environment (relative humidity > 70%) and is probably the minimum to observe Mg²⁺ dissolution and the subsequent hydration processes. This model system is also motivated by a heat storage technology using the MgO hydration reaction.^{5–7,32} The previous computational studies of the hydration^{30–32,47} have relied on pre-assumed reaction pathways, leaving the molecular mechanisms of this slow (hours to days^{7,28,36}) process unclear. In this work, to go beyond the previous works and elucidate the reaction mechanism, we use an advanced molecular simulation method, potential-scaling molecular dynamics (PS-MD), and first-principles calculations, and examine locally stable structures along the hydration without any *a priori* assumptions. This paper begins with an overview of the interfacial structural changes along the hydration. We then investigate the molecular details by classifying the observed structures into three different stages: (1) water adsorption on the MgO surface, (2) Mg²⁺ dissolution into the water layers, and (3) Mg(OH)₂ nucleation. In the first stage, we examine the interfacial water structure, including its HB networks and molecular orientations, to elucidate the mechanism of water dissociation under ambient conditions. In the second stage, mainly representing the initial Mg²⁺ dissolution, we analyze how

this process occurs and identify the origins of its exothermicity by calculating the corresponding energy profiles. Finally, by investigating the third stage, we provide molecular insights into the nucleation and growth of Mg(OH)_2 . Our results suggest that the dissolution-precipitation mechanism is favored over the solid-state reaction mechanism in this system. To the best of our knowledge, this is the first computational study showing that the well-ordered Mg(OH)_2 nanosheets can form from an amorphous precursor phase in an aqueous solution.

2 Computational Methods

This section briefly describes the computational methods used in this study. Full details regarding the methods and validations are provided in Supporting Information.

We first generated various structures relevant to the hydration of MgO using the PS-MD simulation method. This simulation method allows us to induce various structural changes, including barrier-crossing processes of chemical bond breaking/forming and atomic migration, by repeating short MD simulations with continuously scaling the potential energy surface.⁵³ The simulation consists of a repetitive cycle in which the potential energy surface is gradually flattened and then restored. As detailed in Section 3, this technique captured key elementary processes, such as the dissolution of Mg^{2+} ions from the surface and the penetration of protons into the bulk. The observation of these events demonstrates that our simulation accesses timescales inaccessible to conventional MD simulations. The present PS-MD simulations were performed using ReaxFF,⁵⁴ a low-cost classical force field that can handle bond recombination. To generate interfacial structures along the hydration, we performed a total of 1,000 PS-MD cycles. From the trajectory of each cycle, we extract the last snapshot, yielding a total of 1,000 structures. These 1,000 structures were then fully optimized using the same ReaxFF potential to identify locally stable minima.

After the PS-MD simulations and the subsequent optimization calculations at the ReaxFF level, the structures were improved using the density functional based tight binding (DFTB) method.⁵⁵ The DFTB method provides a semi-empirical electronic structure calculation that is two to three

orders of magnitude faster than density functional theory (DFT) calculations. Furthermore, for all structures that were more stable than the initial structure in the DFTB calculations, a further refinement using the more accurate DFT method was performed to select the structures to be analyzed for the hydration. We adopted the BLYP exchange-correlation functional, which has been very widely used in various researches from materials science to life science and is known to perform well in hydrogen-bonded systems.^{21,22,56}

The simulation system was the same for the three calculation levels (ReaxFF, DFTB, and DFT). The solid surface was modeled as a five-layer MgO slab with the perfect (100) surface. In order to investigate the hydration reaction, a water film of two-monolayer thickness was placed on the MgO slab surface. The size of the slab in the lateral xy plane was $16.85 \text{ \AA} \times 16.85 \text{ \AA}$ based on the experimental lattice constant of MgO (4.21 \AA ⁵⁷), and the thickness of the slab, including the water film, was about 17 \AA . Using this simulation system, we performed five independent runs, each consisting of a PS-MD simulation followed by geometry optimizations at the ReaxFF, DFTB, and DFT levels. In the next section, we will investigate the molecular mechanism of the hydration on the basis of the MgO/water interfacial structures finally obtained by the DFT calculations.

3 Results and Discussion

3.1 Overview of the MgO hydration process

First, we overview the MgO/water interfacial structural changes obtained from the calculations. Figure 1 shows results from a representative run: the interfacial structures (upper panels) and the distributions of the z coordinate for Mg, O, and H atoms (lower panels) with respect to the PS-MD cycle. The distributions calculated from the other four runs are shown in Figure S4. In the initial state (PS-MD cycle ~ 0), the presence of two water monolayers is evident from the two distinct peaks in the oxygen distribution at $z > 0$ (Figure 1a). The first water layer on the MgO surface ($z \sim 2.25 \text{ \AA}$) is shown by a very sharp peak, while the second water layer in contact with the gas phase is extended over a wide range in the z direction. This densely packed first layer in the

z direction is consistent with previous studies.^{58,59} The orientation of the water molecules in the first layer can be roughly seen from the distribution of hydrogen. The hydrogen peak appears to be at almost the same position as the oxygen peak, indicating that many water molecules orient their molecular planes parallel to the MgO surface. The hydrogen peak at the slightly higher z coordinate represents water molecules with an HB to molecules in the second water layer, and another hydrogen peak between the top surface of the solid MgO and the first water layer ($z \sim 1$ Å) represents H atoms (or protons) dissociatively adsorbed on the MgO surface. Around the 50th PS-MD cycle (Figure 1b), the small Mg peak appears at the first water layer, indicating that there are Mg²⁺ ions dissolved from the surface. Therefore, we found that the dissolution of Mg²⁺ ions is the first elementary process following the dissociative adsorption of water molecules. Around the 100th PS-MD cycle (Figure 1c), as the dissolved Mg²⁺ ions increase, protons penetrate into the solid, which implies that the two molecular processes are correlated to each other. From the ~ 150 th PS-MD cycle (Figure 1d), we can see the Mg²⁺ ions beginning to dissolve in the second water layer. The layer structure throughout the MgO/water interface is maintained even after the ~ 150 th PS-MD cycle (Figure 1e and 1f) although there are minor changes in the distribution. As these structural changes progress, the potential energy of the system generally decreases (see Section 2 in Supporting Information), which is in qualitative agreement with the exothermic nature of MgO hydration. Further details in Supporting Information show that the system eventually reaches an approximately 64% hydrated state from a potential energetic standpoint.

To quantitatively evaluate these interfacial rearrangements, we count the number of the respective ions along the PS-MD cycle. Figure 2a shows the changes in the number of Mg²⁺ ions dissolved from the MgO surface and the number of protons (H⁺) adsorbed on (or penetrated into) the MgO solid. The dissolved Mg²⁺ and adsorbed protons are defined as ions at $z > 1.25$ Å and at $z < 1.75$ Å, respectively. The number of the protons at the PS-MD cycle zero indicates the number of water molecules dissociated in the initial state. We find from the figure that the dissolved Mg²⁺ ions increases monotonically along the PS-MD cycle and the protons are generated roughly in parallel with Mg²⁺ dissolution. The number of penetrated protons is approximately twice that of the

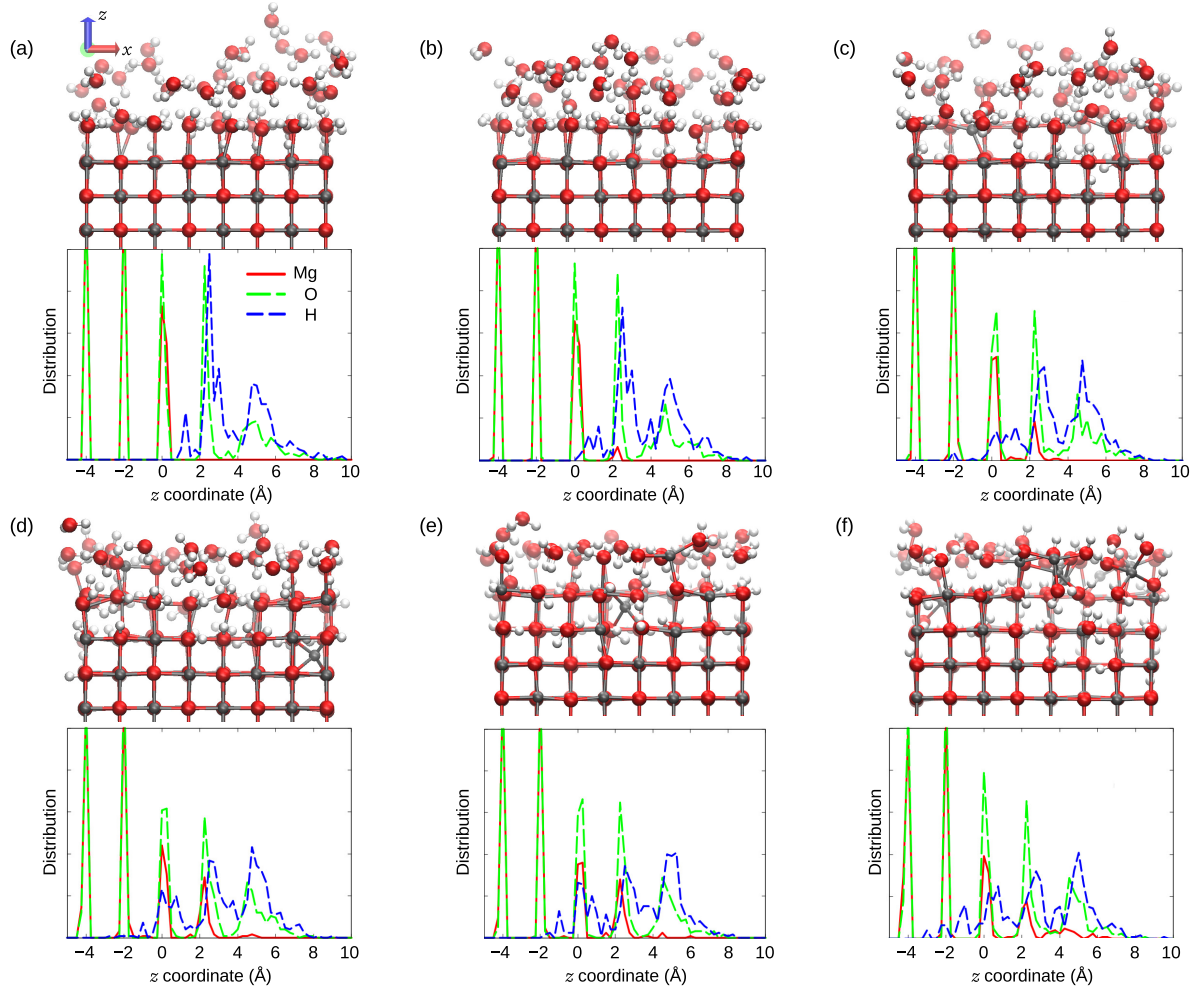


Figure 1: Representative MgO/water interfacial structures optimized at the DFT level (upper panels) and their corresponding z coordinate (\AA) distributions for Mg, O, and H atoms (lower panels) at various stages of the PS-MD cycle. The structures in the upper panels are optimized geometries from specific PS-MD cycles: (a) 0, (b) 45, (c) 92, (d) 162, (e) 205, and (f) 310. The distributions in the lower panels are averaged over five structures within the respective PS-MD cycle ranges: (a) 0–32, (b) 41–47, (c) 88–97, (d) 156–162, (e) 201–205, and (f) 306–310. In the upper panels, Mg, O, and H atoms are colored gray, red, and white, respectively, while, in the lower distribution plots, the lines for Mg, O, and H are red, green, and blue, respectively. Both panels display the interface above the second MgO layer from the bottom. Bonds between Mg and O atoms are shown for distances shorter than 2.3 \AA . The z coordinate is measured relative to the peak position of the outermost MgO layer.

Mg^{2+} ions. This is a result that the charges of the Mg^{2+} ions in the solid have been compensated by the protons, suggesting that the proton penetration correlates with the Mg^{2+} dissolution process. This observation appears to be consistent with a suggestion by Wogelius *et al.* who proposed the solid-state reaction mechanism in nucleation and growth.³⁴ In the particularly early cycle (before the ~ 100 th PS-MD cycle), many Mg^{2+} ions are dissolved during the short period owing to the initially hydroxylated sites on the MgO surface. After the ~ 100 th PS-MD cycle, when about one thirds of the surface Mg^{2+} ions have been dissolved, the dissolved Mg^{2+} ions on the surface begin to migrate into the second water layer (blue plot in Figure 2a). This migration reduces the ions on the surface, which probably induces further dissolution of Mg^{2+} ions from the surface.

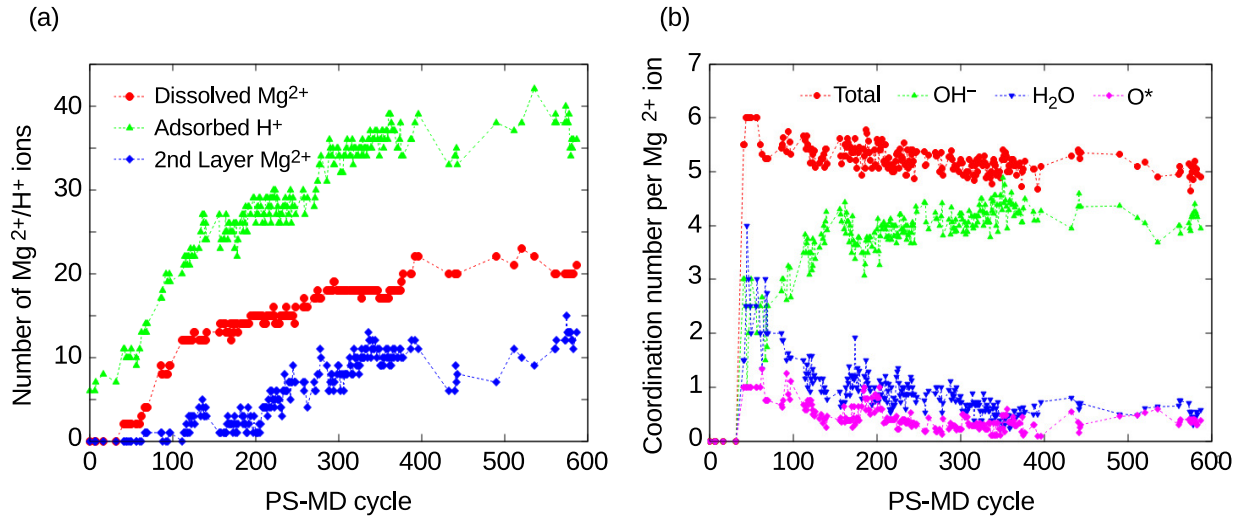


Figure 2: (a) Number of dissolved Mg^{2+} ions (red) and adsorbed/penetrated protons (green) along the PS-MD cycle. The number of Mg^{2+} ions in the second water layer (blue), whose z coordinates are greater than 2.75 \AA , is also shown. (b) Coordination number of dissolved Mg^{2+} ion along the PS-MD cycle. The total coordination number is shown in red, and contributions to that from OH^- (green), H_2O (blue), and MgO surface oxygen atoms (O^* ; magenta) are also shown. The dotted lines are guides for the eye. Similar results from the other four runs are presented in Figures S6 and S7. Note that data points are not shown for PS-MD cycles where the optimized structure is less stable than the initial one (see Section 2 in Supporting Information for details).

To examine how the dissolved Mg^{2+} ions are stabilized, we then analyze the evolution of their

local coordination environment. Figure 2b shows the change in oxygen species, OH^- ion (green), H_2O molecule (blue), and surface oxygen atom O^* (magenta), coordinated to the dissolved Mg^{2+} ions. We found that the dissolved Mg^{2+} ion is typically coordinated with more than five oxygen atoms (red plot in Figure 2b). At an early stage (\sim 50th PS-MD cycle), the dissolved Mg^{2+} ions are stabilized by both OH^- and H_2O species at equal ratio. Note that, at this stage, a surface oxygen always coordinates to the dissolved Mg^{2+} ions because they reside on the MgO surface. As the PS-MD cycle proceeds, the coordination of H_2O molecules is replaced with OH^- ions. Eventually (\sim 300th PS-MD cycle), the OH^- ion bears \sim 80% of the total coordination. The increase in the coordination by OH^- ions is definitely related to the consecutive water dissociation that occurs at the MgO /water interface (see Figure S8 for the z coordinate distributions of oxygen species). The observation that OH^- ions form at the interface is also reported by Ončák *et al.*³¹

Based on the results in this section, the obtained structures can be classified qualitatively into three stages according to the Mg distribution change (Figure 1): (1) the initial stage where water molecules are dissociatively adsorbed and no Mg^{2+} ions are dissolved (around the 0th PS-MD cycle), (2) the stage where Mg^{2+} ions are dissolved into the first water layer on the MgO surface (around the 50th PS-MD cycle), and (3) the stage where Mg^{2+} ions permanently exists in the second water layer (after around the 100th PS-MD cycle). In the following sections, we examine the interfacial structures of these three stages in detail, using all optimized structures obtained from the five independent runs.

3.2 Dissociative adsorption of water molecules

First, we investigate the structure and dissociative adsorption of water at the first stage, which represents the initial state of the MgO hydration reaction and serves as the precursor to Mg^{2+} dissolution. Our primary focus is to understand the dissociation of water molecules on the basis of the HB networks at the interface and the orientation of water molecules. The dissociation ratio of the surface water molecules was calculated to be 20%. While various dissociation ratios have been reported in the literature, ranging from 0% to 75%,^{21,25,27,31,33} our result is in good agreement

with the result of *ab initio* molecular dynamics by Ding and Selloni (22%).⁵⁹ Figure 3a shows the distribution of the number of HBs per water molecule. Hydrogen bonds were defined using the geometric criteria by Luzar and Chandler.⁶⁰ Water molecules in the first layer on the MgO surface (represented by red) predominantly form three HBs, fewer than in bulk water (3.7 HBs per molecule).^{61,62} This difference can be attributed to the fact that these water molecules reside directly on the MgO surface. The oxygen atoms of the interfacial water molecules can be positioned atop Mg sites (Figure S9) because the distance between nearest-neighbor surface Mg (Mg^*) atoms ($\sim 2.98 \text{ \AA}$) is roughly similar to the typical oxygen-oxygen distance in hydrogen-bonded water molecules ($\sim 2.78 \text{ \AA}$). Also, the average distance between these Mg^* atoms and the O atoms of the water molecules is $\sim 2.2 \text{ \AA}$, indicating a strong electrostatic interaction. Therefore, the coordination environment of the first-layer water molecules effectively consists of three HBs and one Mg^* -O bond. While this four-fold coordination agrees well with that of bulk water, the geometric structure is significantly different; Bulk water generally favors a tetrahedral coordination geometry, whereas the tetrahedral geometry for these first-layer molecules is highly distorted (Figure S10a).

This distorted structure of interfacial water is associated with their specific orientations on the interface. Figure 3b shows a two-dimensional probability distribution based on two angles: θ , the angle between the dipole moment vector of the water molecule and the z axis (normal to the MgO surface), and φ , the angle between the vector connecting the two hydrogen atoms of the water molecule and the z axis. The most prominent peak corresponds to $(\theta, \varphi) \sim (90^\circ, 90^\circ)$, indicating a dominant lying-down orientation where the plane of the water molecule is oriented parallel to the MgO surface. In addition, weaker peaks are observed around $(\theta, \varphi) \sim (50^\circ, 70^\circ)$ and $(\theta, \varphi) \sim (50^\circ, 110^\circ)$. These represent upward orientations, where the dipole moment is directed toward the gas phase ($\theta < 90^\circ$). Water molecules with the lying-down orientation participate in a two-dimensional HB network within the first water layer, whereas those with the upward orientation participate in the two-dimensional HB network while also forming HBs with molecules in the second water layer. Such HB networks and molecular orientations imply that specifically oriented (i.e., downward-oriented) water molecules dissociate. Interestingly, the downward ori-

tation, where the dipole moment points toward the MgO surface, was rarely observed (Figure 3b). This scarcity is likely due to the dissociation of these downward-oriented molecules, triggered by strong interactions with their neighbors. Indeed, the resulting hydroxide ions, similar to the water molecules, adopt a lying-down or upward orientation (Figure S10b). That is, it is water molecules adopting a downward orientation, for instance due to thermal fluctuations, that are promoted to dissociate by the surrounding HB network. This dissociation mechanism is consistent with the observed interatomic distances and configurations. The average O-H bond length of the interfacial water molecules was longer (1.003 Å) than that of the isolated water molecule (0.979 Å) (Figure S11a), suggesting that they are primed for dissociation. Critically, we observed short and strong HBs between dissociated hydroxide ions and adjacent water molecules (Figure S11b). These HBs appear in configurations, typified by Figure 3c, where an adsorbed proton is located beyond the HB between the hydroxide ion and the water molecule (green dotted line). Such configurations strongly suggest that the downward O-H bond dissociates (the proton is pushed out) by the strong HB donor of a neighboring water molecule from the opposite side.

On the other hand, the second water layer on the gas phase seems to possess a water structure more similar to bulk water than the first layer. Figure 3a shows that, in the second layer, the average number of HBs per water molecule is 3.7, which is quite similar to that of bulk water (3.7). The orientation of water molecules appears largely random although the downward orientation is slightly increased due to the HB with molecules in the first layer (Figure S12). The tetrahedrality is also considerably closer to that of bulk water compared to the first layer (Figure S10a). In fact, these characteristics have been suggested in previous studies.^{58,63} Nevertheless, a number of molecules are found to deviate from the tetrahedral structure given that there are water molecules with small or even negative tetrahedral order parameters (Figure S10a). The deviation from the tetrahedral structure likely results from the molecules' effort to maintain HBs even on the gas phase. While Laporte *et al.* described the water in the second layer as the bulk-like water because the O-O distance in hydrogen bonded pairs is quite close to that of bulk water,⁵⁸ our results suggest that distorted structures allow the molecules to maintain such O-O distances even in the different

environment from the bulk. Note that, in contrast, Ding *et al.* suggested on the basis of the molecular diffusion that the bulk-like behavior begins from the third layer.⁵⁹

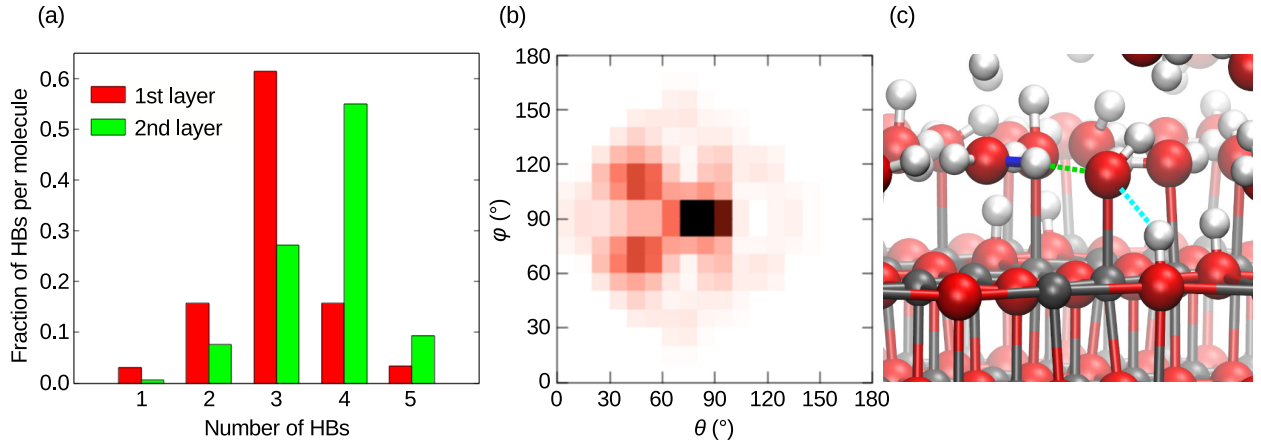


Figure 3: (a) Fraction of the number of hydrogen bonds (HBs) per molecule in the first (red) and second (green) water layers. (b) Two-dimensional probability distribution of the orientation angles θ (°) and φ (°), for water molecules in the first layer, where a darker color indicates higher probability. (c) Key hydrogen-bonded configuration involved in water dissociation. In panel (c), the blue bond represents the elongated O-H bond (1.05 Å), while the green (1.54 Å) and cyan (2.20 Å) dotted lines represent the HBs within the $\text{H}_2\text{O}\cdots\text{OH}^-\cdots\text{HO}^*$ complex. Note that the oxygen and hydrogen atoms connected by the cyan dotted line originally formed the downward O-H bond of a single water molecule before its dissociation.

3.3 Dissolution of Mg^{2+} ions

The second stage spans from the first observation of the Mg^{2+} dissolution process until just before Mg^{2+} ions are constantly present in the second water layer. In this period, roughly 10 Mg^* atoms (about 30% of the surface Mg atoms) are dissolved (Table S2). In this section, we mainly examine the initial Mg^{2+} dissolution process. According to the structures optimized at the DFT level, the dissolved Mg^{2+} ions are typically located on top of O^* sites. As depicted in Figures 1b and 1c, their z coordinates (~ 2.25 Å) are comparable to those of the oxygen atoms in the first water layer. This observation that most of the dissolved Mg^{2+} ions are found above O^* sites implies that the fully hydroxylated MgO surface during the first stage hinders the subsequent elementary process of Mg^{2+} dissolution. Most of these Mg^{2+} ions on top of O^* sites exhibit an octahedral six-coordinate

structure (Figure 4a). These solvated ions include what Ončák *et al.* described as a contact ion pair.³¹ On the other hand, a few dissolved Mg^{2+} ions are observed bridging two O^* sites at $z \sim 1$ Å with the low octahedrality, making them unstable compared to the five- or six-coordinate Mg^{2+} ions. (see below for details). Note that in the present calculations no H^+ penetration was found before Mg^{2+} dissolution in contrast to the suggestions by previous works.^{34,35}

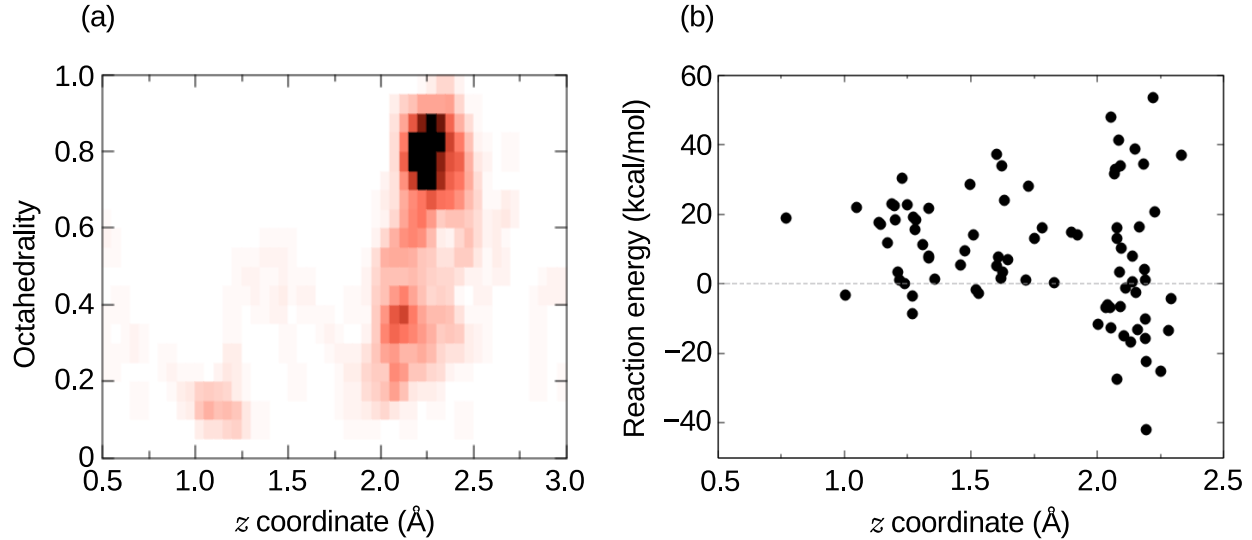


Figure 4: (a) Two-dimensional probability distribution of the octahedral order parameter⁶⁴ for the solvated Mg^{2+} complex as a function of its z coordinate calculated by the five independent runs. A darker color indicates higher probability. (b) Reaction energy (kcal/mol) plotted against the z coordinate of the Mg^{2+} ion obtained from the nudged elastic band calculations. Only dissolution processes with a locally stable product structure are used.

Our focus in the second stage is what causes the exothermic dissolution of Mg^{2+} ions. Unfortunately, however, the structures optimized at the DFT level represent only fragmented local stable points, and it is difficult to examine the reaction pathway and its corresponding energy profile. Therefore, we performed nudged elastic band (NEB) calculations to determine the dissolution pathway for each surface Mg^{2+} ion, using the final configuration from the first stage as the reactant. The calculation generates a total of 160 independent dissolution pathways, arising from 32 surface Mg^{2+} ions for each of the five independent runs (see Supporting Information for the computational details). We counted the Mg^{2+} ion with the z coordinate greater than 0.75 Å in the

product as the successfully dissolved Mg^{2+} ion. This criterion was met by 83 Mg^{2+} ions, while for the remaining 77 ions, no stable dissolved state was found; the latter ions returned to the solid surface. This observation indicates that the successful dissolution process is highly dependent on the local environment of water molecules. Furthermore, among the 83 samples where the dissolution was observed, only 25 samples exhibited an exothermic (negative) reaction energy. The resulting energy profiles of the dissolution processes are presented in Figure S13. For the dissolution processes with a negative reaction energy, the average reaction barrier relative to the reactant was found to be $\sim 12 \pm 12$ kcal/mol. This barrier height is comparable to the activation energy of $\sim 13\text{--}18$ kcal/mol reported in previous studies^{39,65,66} that suggested Mg^{2+} dissolution or interfacial reactions as the rate-determining process. The significant variation of the calculated barrier height reflects the severely heterogeneous nature of this process. Also, this barrier is not so high, indicating that the dissolution can occur exothermically even in the perfect (defect-free) MgO (100) surface, not necessarily at the edge.

The above observation raises questions of which product structures favor exothermic dissolution and what drives this process. Our analysis revealed a correlation between the reaction energy and the z coordinate of the dissolved Mg^{2+} ion (Figure 4b). Specifically, the dissolution process tends to be exothermic when the Mg^{2+} ion is positioned 2.0 Å or greater from the surface. Given that Mg^{2+} ions in this region tend to adopt an octahedral structure (Figure 4a), the product is expected to be stabilized by sufficient coordination. Thus, for the dissolution to be energetically favorable, it is crucial that the Mg^{2+} ion positions itself directly above an O^* site to form the octahedral structure. However, such Mg^{2+} ion's position and an octahedral structure do not guarantee a negative reaction energy. Therefore, we further classified the product structures where the z coordinate of the Mg^{2+} ion is 2.0 Å or greater.

Figure 5a presents a box plot of the reaction energy classified by the number of ligands (H_2O or OH^-) coordinated to the dissolved Mg^{2+} ion. It should be noted that since the dissolved Mg^{2+} ion is positioned on an O^* atom, the coordination number of five in the figure denotes a total coordination number of six, including the O^* atom. Although the variation in the reaction energy is

quite substantial, both the mean (red circle) and median (horizontal bar in the box) values of the reaction energy tend to decrease as the number of ligands increases. This indicates that the dissolved Mg^{2+} ion is stabilized by coordination with water molecules and hydroxide ions. However, even with total six-coordination allowing for an octahedral structure, a negative reaction energy is not guaranteed. Conversely, configurations with a total coordination number of four or five can still yield negative reaction energies. This raises the next question; is there another structural feature of the products that strongly correlates with the reaction energy? The stability of the product also depends on how significantly a vacancy, which is created at the original position of the dissolved Mg^{2+} ion, is stabilized. The role stabilizing the vacancy is played by protons adsorbed on nearby O^* sites. Figure 5b classifies the reaction energy according to the number of these protons surrounding the vacancy. Again, we can observe a trend that the reaction energy decreases as the number of the protons increases. According to formal charge considerations, two protons can largely neutralize the electrostatic instability (i.e., repulsive interaction between the O^* atoms around the vacancy) caused by Mg^{2+} dissolution. Ončák and co-workers called this neutralizing process "defect healing".²⁷ Indeed, a rough boundary between the positive and negative reaction energies seems to lie between having one and two protons. Notably, within our samples, all product structures with three protons infilling the vacancy show negative reaction energies. Compared to the classification by the coordination number of the Mg^{2+} ion (Figure 5a), the classification by the number of surrounding protons exhibits smaller variance and fewer outliers relative to the median. Therefore, we suggest that the stabilization of the vacancy is particularly crucial for achieving a favorable dissolution structure. In addition, once an Mg^{2+} ion dissolves and the vacancy is occupied by protons, the ion's return to the surface becomes infeasible; the process is effectively irreversible. Finally, Figure 5c classifies the reaction energy according to the combined count of the coordinating ligands and the protons infilling the vacancy. As expected, the clearer trend can be found that the stability of the product increases with a larger total number of these species.

DFT calculations not only provide plausible molecular interfacial structures but also offer insights into the electronic states. Figure 5d shows how the projected density of states (pDOS) of

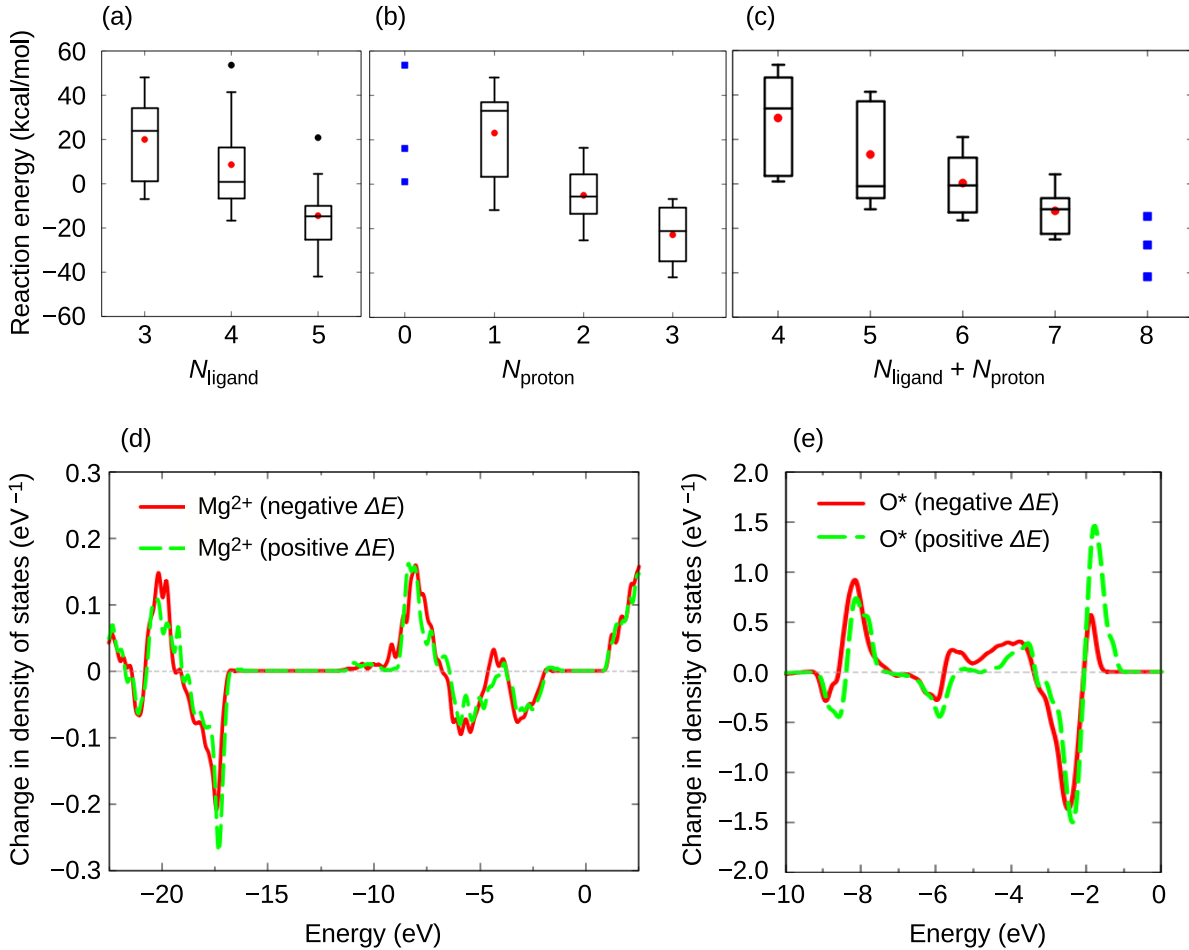


Figure 5: (Upper) Boxplot of the reaction energy (ΔE , kcal/mol) for the Mg^{2+} dissolution process classified by (a) the number of ligands (OH^- ions and H_2O molecules) coordinated to the dissolved Mg^{2+} ion, N_{ligand} , (b) the number of protons adsorbed on O^* atoms adjacent to the vacancy generated by the dissolution, N_{proton} , and (c) the sum of the number of the ligands and protons. The distance cutoffs for Mg^{2+} -O coordination and O^* -H⁺ bonding are set to 2.5 Å and 1.2 Å, respectively. The red and black circles indicate mean reaction energy and outlier in the category, respectively, and the blue squares are used when there are less than four samples. (Lower) Change in the projected density of states of the dissolved Mg^{2+} ion (d) and the O^* atoms originally coordinated to the dissolved Mg^{2+} ion (e) for the dissolution process. The density of states of the Mg and O^* atoms are projected onto their (3s, 3p) and (2s, 2p) orbitals, respectively. The changes according to the process with negative and positive reaction energies are colored red and green, respectively. In both panels, the reference energy is set to the vacuum level in the slab model.

the dissolving Mg^{2+} ions ($z > 2.0 \text{ \AA}$) changes in the dissolution process. (The pDOS changes of the O atoms coordinating to a dissolving Mg^{2+} ion are shown in Figure S14.) The red solid and green dashed lines correspond to the changes in pDOSS obtained from the dissolution processes with negative and positive reaction energies, respectively. We found that high-energy occupied states at about -5.5 eV and -3.0 eV diminish and largely shift to a lower energy region around -8.0 eV . This is a consequence of the change in the chemical state of the Mg^{2+} ion as its coordination changes from bonding with O^* atoms to coordination with H_2O and OH^- ligands (Figure S15). This stabilization of the one-electron state can be one of the driving forces for the dissolution process (cf. Figure 5a). However, this feature is almost unchanged between exothermic and endothermic dissolution processes. Figure 5e shows, on the other hand, the change in pDOSS of the O^* atoms originally coordinated to the dissolving Mg^{2+} ion. Although similar pDOS changes appear to be observed regardless of the reaction energy, a significant difference is apparent around -1.9 eV . In the case of processes with a positive reaction energy, the pDOS at -1.9 eV substantially increases (green dashed line), whereas the increase is considerably smaller for a negative reaction energy (red solid line). In the former case, a large portion of the state at -2.5 eV is found to shift to -1.9 eV , which corresponds to the dissolution process where the O^* atoms fail to be stabilized by the proton adsorption. The stabilized O^* states, in contrast, can be seen around a lower energy region ($-6 \text{ eV} \sim -4 \text{ eV}$), which is related to the dissolution process with a negative reaction energy. Therefore, this increase in the pDOS at -1.9 eV reflects the fact that the O^* atoms are not stabilized by protons during the dissolution process. These results indicate that the suggestion from Figure 5a-c is also supported from the viewpoint of electronic states; the proton adsorption on the O^* atoms plays an important role in the exothermic dissolution process.

Understanding the exothermicity from a viewpoint of the reactant structure is not straightforward in the Mg^{2+} dissolution process. Since the product structure infilling the vacancy is expected to be intimately related to the hydroxylation around the Mg^* atom to be dissolved in the reactant state, the latter would be linked to the exothermicity of the reaction. However, we found no significant correlation between the number of hydroxylated O^* atoms and the reaction energy (Figure

S16). This is because the slight displacement of the Mg^{*} atom significantly changes the orientation of surrounding hydroxide ions and water molecules, and consequently triggers water dissociation or proton transfer. Indeed, Hu and co-workers have reported that the energy barrier is small for proton transfer among water molecules and hydroxide ions on the MgO surface.⁶⁷ Therefore, our results indicate that Mg²⁺ dissolution is a concerted process coupled with rearrangements of the local HB network. This implies that a detailed analysis of the HB network is necessary to understand the exothermic Mg²⁺ dissolution from a viewpoint of the reactant structure. According to the present static calculations, the range of proton transfer is limited to the second hydration shell of the Mg²⁺ ion, suggesting that an analysis of a relatively local network is sufficient. This static picture is potentially modified by dynamic fluctuations, which could extend the influence from the Mg²⁺ ion displacement.

3.4 Nucleation and growth of Mg(OH)₂

The third stage of the present hydration process represents states where dissolved Mg²⁺ ions are persistently located in the second water layer (i.e., after around the 100th PS-MD cycle). Here, we focus on the formation of Mg-OH chains relevant to the Mg(OH)₂ nuclei and show the possibility of two previously suggested nucleation and growth mechanisms.

One is the solid-state reaction mechanism, wherein an Mg(OH)₂(0001) layer forms on the MgO (111) surface. To investigate this mechanism, we examined proton penetration through vacancies created by Mg²⁺ dissolution. At approximately the 300th PS-MD cycle (the approximate limit for the structural analysis herein; see Section 2 in Supporting Information for details), eight protons on average have penetrated into the first sublayer (Figure S17). This quantity corresponds to one-quarter of the O atoms in that layer. These penetrated protons bind to O atoms, compensating for the charge of the dissolved Mg²⁺ ions. Consequently, the O atoms in the solid largely remain in their original sites, which is consistent with the early experimental study by Wogelius *et al.*³⁴ The resulting OH⁻ ions are distributed on the surface and in the first sublayer (Figure S18), forming rows on the (111) plane of the MgO crystal that align along the [110] direction. This configu-

ration is consistent with the molecular hydration process proposed by Jug *et al.*³⁰ However, this process stalled almost completely at the first sublayer (Figure S17). For proton penetration to proceed deeper, Mg^{2+} ions must dissolve from the second sublayer, but such dissolution was hardly observed. This is because the Mg^{2+} ions in the second sublayer are strongly stabilized by the persistent MgO lattice framework (i.e., lattice potential dominated by Madelung potential). Thus, it is highly unlikely that a large $Mg(OH)_2$ film forms in the solid by the proton penetration as long as the MgO solid framework is maintained. This implies that if a solid-state reaction mechanism were to be assumed, the extraction of internal Mg^{2+} ions would become the rate-determining process. This implication is consistent with the findings of Ishida and Ishimura.³²

An alternative pathway using the MgO (111) plane may be to form [110] steps and gradually expose underlying (100)-oriented terraces. This surface reconstruction requires the continuous dissolution of surface Mg atoms, which in turn allows for the construction of OH^- rows in the newly exposed deeper regions (a schematic illustration of this process is shown in Figure S19). However, the resulting structure would slightly differ from the stable $Mg(OH)_2$ structure. For example, since the OH^- rows are constrained by the strong lattice potential from the underlying $MgO(111)$ plane, they are forced to adopt an O-O distance of ~ 2.98 Å similar to that in the MgO crystal. This distance is inconsistent with the ~ 3.15 Å distance found in a relaxed $Mg(OH)_2$ structure. As long as the substrate maintains the MgO rock-salt structure, this lattice mismatch makes structural relaxation difficult, leading to energetically unfavorable and strained structures.

The other possible nucleation and growth is the formation of $Mg(OH)_2$ via dissolution, aggregation, and precipitation. When Mg^{2+} ions dissolve and move away from the MgO surface, they experience a weaker lattice potential. (Ončák *et al.* seem to refer to these ions as a solvent-separated ion pair.³¹) Figure 6a illustrates the lateral distribution of Mg^{2+} ions situated on the MgO surface, with the z coordinates ranging from 1.0 Å to 3.0 Å. These ions are clearly well-aligned on O^* sites with a strong influence from the underlying MgO lattice. These aligned ions can form structures corresponding to energetically stable stripe configurations described by Ončák *et al.*^{27,31} In contrast, Figure 6b shows that Mg^{2+} ions with the z coordinates of 3.0 Å or greater

are distributed more randomly in the xy plane. This is attributed to the fact that these Mg^{2+} ions are coordinated purely by water molecules or hydroxide ions. This difference in the local environment is also reflected in the local structure. Figure 6c shows the bond angle distribution for $\text{O}(\text{-H})\text{-Mg-O}(\text{-H})$ chains observed in the third stage. The distribution for the chains on the MgO surface (red) exhibits sharp peaks around 90° and 170° . This serves as evidence that the influence of the MgO rock-salt structure remains significant. We found from the green plot, obtained from the chains in the second water layer ($z > 3.0 \text{ \AA}$), that this strong influence from the MgO crystal diminishes. Although a peak is present at 90° , its intensity is reduced, and structures characterized by wider bond angles ($100^\circ\text{-}120^\circ$) become more prevalent. In addition, the peak at 170° changes to a shoulder. Such lateral positions and local structures surrounding Mg^{2+} ions that are less affected by the MgO lattice potential are more pronounced at the outermost interface (Figures S20 and S21).

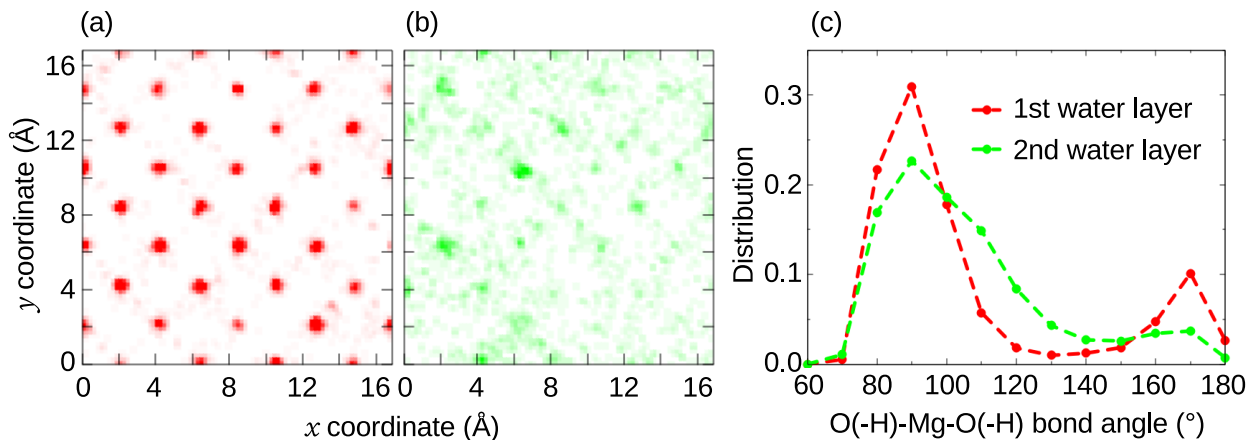


Figure 6: Normalized lateral distribution of dissolved Mg^{2+} ions in the (a) first ($1.0 \text{ \AA} < z < 3.0 \text{ \AA}$) and (b) second ($z > 3.0 \text{ \AA}$) water layers. (c) Bond angle distribution of $\text{O}(\text{-H})\text{-Mg-O}(\text{-H})$ chains found in the first (red) and second (green) water layers. In both panels, the Mg^{2+} ions are sampled from snapshots in the third stage.

Figure 7a presents a typical example of Mg-OH chains found in the second water layer. The chain comprises five dissolved Mg^{2+} ions and they are interconnected solely by OH^- ions, without any water molecules or surface oxygen atoms. In Figure 7b, the Mg-OH chain is extracted from

the interface and viewed from a different angle. This structure is found to have a morphology reminiscent of $\text{Mg}(\text{OH})_2$ crystals (shown in Figure 7c). This calculation result suggests, based on their structural similarity, that the Mg-OH chains in regions far from the MgO surface can be precursors of $\text{Mg}(\text{OH})_2$ crystal nuclei. Such Mg-OH chains are likely the surface clusters or amorphous phases experimentally observed on MgO crystals.^{36,44,50,68}

However, the Mg-OH chains found in the present calculation contain four- and five-coordinate Mg^{2+} ions, unlike the uniformly six-coordinate Mg^{2+} ions within the crystalline $\text{Mg}(\text{OH})_2$. The primary reason for this incomplete coordination is the thinness of the water layer. For Mg^{2+} ions to dissolve from the MgO surface, achieve adequate solvation, and establish their preferred coordination by OH^- ions, the space provided by an initial two-layer water film is insufficient.⁵¹ Indeed, the upper part of the Mg-OH chain shown in Figure 7a is exposed to the gas phase, while some of its lower OH^- ions are located on the MgO surface. Therefore, to gain further evidence for the mechanism of $\text{Mg}(\text{OH})_2$ crystal nuclei formation far from the MgO surface, we require additional simulations involving a more substantial number of water molecules.

In order to demonstrate that the nucleation and growth of $\text{Mg}(\text{OH})_2$ occurs in an environment with sufficient water molecules, we performed the additional simulations mentioned above. We extracted an amorphous phase consisting of Mg, O, and H atoms on the MgO surface ($z > 1 \text{ \AA}$), placed it in bulk water, and performed PS-MD simulations and subsequent geometry optimizations at the DFTB and DFT levels (see Supporting Information for computational details). As a result, we successfully obtained crystalline Mg-OH chains exhibiting an $\text{Mg}(\text{OH})_2$ -like structure (Figure 8). We find from the figure that eight Mg^{2+} ions form a two-dimensional layered structure, and the bridging OH^- ions are arranged in positions that precisely match those in the $\text{Mg}(\text{OH})_2$ crystal structure (Figure 7c). This structure is considerably more well-ordered compared to the Mg-OH chains observed in the MgO/water interface system (Figure 7b). The aqueous environment without the MgO lattice potential likely contribute to the formation of this well-ordered crystal nucleus. In the present calculations, the further growth of this $\text{Mg}(\text{OH})_2$ crystal nucleus was not observed. To achieve such growth, we would need more refined adjustments to the potential scaling param-

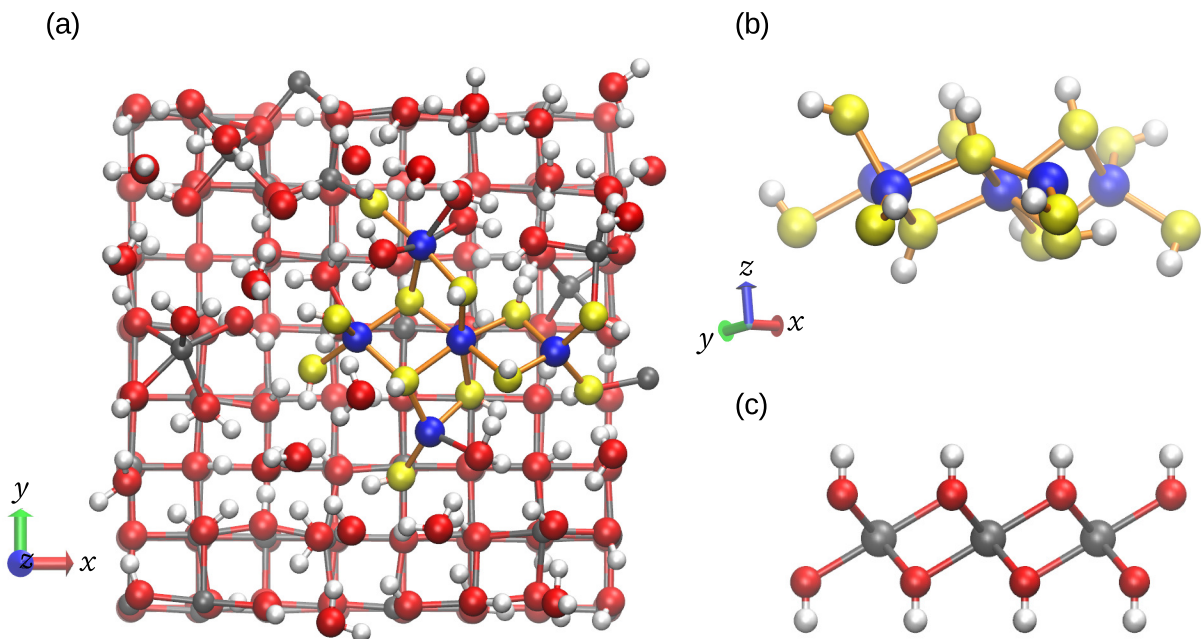


Figure 7: (a) Representative MgO/water interfacial structure with an Mg-OH chain far from the MgO surface. The Mg and O atoms of the chain are highlighted by blue and yellow, respectively, and the other Mg and O atoms are colored gray and red, respectively. The H atoms are colored white. (b) The Mg-OH chain seen from another angle, which is similar in morphology to part of the $\text{Mg}(\text{OH})_2$ crystal displayed in panel (c).

eter and longer simulation durations in the PS-MD simulations. Elucidating the nucleus growth through such simulations remains a task for future work. Nevertheless, the present calculation results clearly support the mechanism that $\text{Mg}(\text{OH})_2$ crystal nuclei dominantly form via dissolution, aggregation, and precipitation in regions far from the MgO surface.

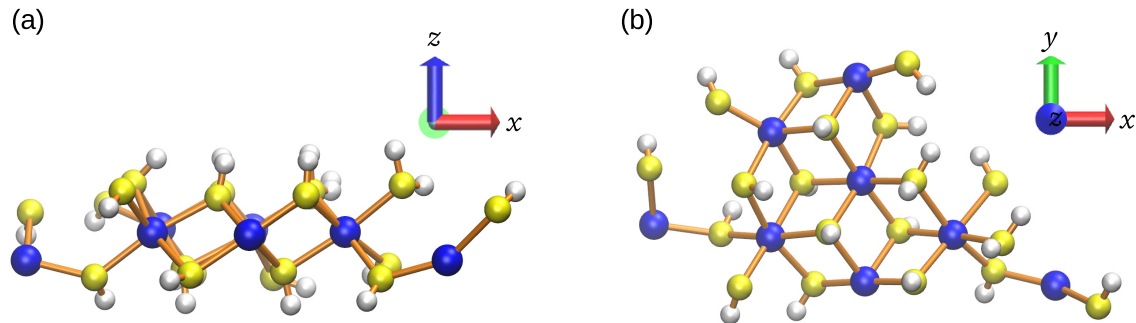


Figure 8: Side (a) and top (b) views of a representative Mg-OH chain obtained in water. The Mg, O, and H atoms are colored blue, yellow, and white, respectively. Surrounding molecules are omitted for clarity.

3.5 Implications on the rate-determining process

Identifying the rate-determining process is a key to understanding the mechanism of complex and multi-step solid-surface chemical reactions. Our investigation focused on two important processes in MgO hydration: the initial dissolution of an Mg^{2+} ion and the nucleation of $Mg(OH)_2$. Our calculations estimated the energy barrier for the dissolution of an Mg^{2+} ion from the defect-free MgO(100) surface to be approximately 12 kcal/mol. According to transition state theory, this barrier height corresponds to a timescale of milliseconds. We did not estimate the barrier height for the subsequent Mg^{2+} dissolution process. However, in the presence of sufficient water, we expect the barrier height to be comparable to or lower than that for the initial one. This is because a surface that has undergone Mg^{2+} dissolution is already disordered and defect-rich. On the other hand, we expect that the nucleation of $Mg(OH)_2$ from a supersaturated aqueous layer is a faster process than the Mg^{2+} dissolution. Because the PS-MD simulations for the nucleation in water were performed under a milder potential scaling condition than that used for the structure generation of the MgO/water interface (see Computational Methods in Supporting Information), the energetic barrier for the nucleation is expected to be lower than that for the Mg^{2+} dissolution. Considering the high concentration of dissolved Mg^{2+} ions in a water layer, the entropic barrier in nucleation is expected to be minimal. Therefore, the rate-determining process, i.e., the elementary process with the highest activation barrier in the overall reaction, is most likely the dissolution of Mg^{2+} ions. This finding is consistent with the experimental results of Kuleci *et al.*, which suggest that the hydration rate is governed by interfacial reactions.³⁹ This implication leads to a seeming discrepancy between the millisecond timescale of this rate-determining process and the hour-long timescale of the macroscopic reaction,^{7,13,43,51,66,69} but it is reconciled by the sequential nature of the reaction. The transformation of the MgO surface is not a single event but requires a long sequence of these dissolution processes to supply sufficient Mg^{2+} ions for the nucleation and growth of a new $Mg(OH)_2$ phase. Therefore, while the individual rate-determining process is fast, the overall reaction rate is determined by the cumulative effect of these sequential dissolutions. This consideration can explain the experimental observation that hydration is much faster on surfaces

with a high density of steps and edges.^{49,66} These defect-rich sites simply lower the activation barrier of the rate-determining process itself. This increases the rate of the individual events, which in turn accelerates the overall sequence and, consequently, the macroscopic reaction rate.

Note that some experimental studies suggest the diffusion of Mg^{2+} ions and water molecules through the product $Mg(OH)_2$ layer on the MgO surface can become rate-limiting.^{14,36,42,50,69} This process, however, governs the later stages of the hydration after the initial precipitation and can be distinguished from the initial rate-determining steps discussed here.⁵⁰ Nevertheless, this subsequent diffusion-limited process is undoubtedly critical for achieving the complete conversion of the MgO solid.

4 Conclusions

We have elucidated molecular processes in MgO hydration by investigating a variety of interfacial structures obtained through a computational chemistry approach, including PS-MD simulations and DFT calculations. In this study, we particularly focused on three fundamental processes of the hydration reaction: the dissociative adsorption of interfacial water, the dissolution of Mg^{2+} ions at the early stage, and the nucleation and growth of $Mg(OH)_2$. Based on the findings of this study, the molecular process of the hydration reaction can be summarized as follows.

First, upon sufficient adsorption, water molecules strongly bound on the MgO surface form a geometrically distorted two-dimensional HB network in the first layer. This HB network triggers the dissociation of downward-oriented water molecules. We have demonstrated that the next step following the dissociative water adsorption is the dissolution of Mg^{2+} ions from the surface. This dissolution can proceed exothermically even from the defect-free surface with an average activation barrier of ~ 12 kcal/mol, indicating that Mg^{2+} dissolution is both thermodynamically and kinetically feasible. However, not all Mg^{2+} ions exothermically dissolve from the surface. In terms of a molecular and electronic structure, the most important factor driving exothermic dissolution was found to be the sufficient stabilization of the resulting vacancy through proton adsorption onto

neighboring oxygen atoms. Thus, the dissolution of Mg^{2+} ions is revealed to be a concerted process, involving not only the coordination by water molecules and hydroxide ions but also the water dissociation. This result also indicates that the dissolution is a highly heterogeneous process that strongly depends on the local HB network structure. Following the initial dissolution of Mg^{2+} ions, the hydration continues with the further dissolution of Mg^{2+} ions and the concurrent penetration of protons into the MgO solid. This proton penetration is crucial for compensating for the negative charge vacancy created by the dissolved Mg^{2+} ions. The dissolution of Mg^{2+} ions from an upper layer opens pathways, facilitating the subsequent Mg^{2+} dissolution from the sublayers. The fate of these dissolved Mg^{2+} ions is twofold: while some are incorporated into a newly formed MgO layer on the original MgO surface, others migrate to the outer water layer. This migration is thought to promote further Mg^{2+} dissolution from the crystal lattice. It is also expected that these newly exposed Mg^{2+} ions attract additional water molecules from the gas phase when the hydration is operated in a humid atmosphere. Finally, $Mg(OH)_2$ nucleation and growth proceeds according to the dissolution-precipitation mechanism rather than the solid-state reaction mechanism. Nucleation and growth via the solid-state reaction mechanism is difficult because it requires the removal of Mg^{2+} ions from the subsurface while maintaining the surrounding MgO (111) layer. This process and the relevant structural relaxation are severely hindered by the strong lattice potential from the MgO crystal environment. In contrast, the dissolution-precipitation mechanism involves Mg^{2+} ions that have moved far enough from the MgO surface to escape the influence of the lattice potential. These solvated ions then combine with OH^- ions within the water layer to form chain-like structures, which act as precursors to the $Mg(OH)_2$ crystal nuclei. This process is greatly facilitated by the presence of sufficient water, as evidenced by the spontaneous formation of a well-ordered crystalline $Mg(OH)_2$ -like nucleus in calculations of a bulk water environment. This result demonstrates that an adequate aqueous environment is essential for efficient nucleation and growth.

Although the hydration of MgO is sensitive to the experimental conditions and is also a non-equilibrium process probably without a single and unique reaction pathway, we have revealed a

series of plausible, locally stable intermediate structures and the relevant molecular processes governing the chemical reaction on its complex energy landscape. We view this work as a foundational step toward computationally elucidating the mechanisms of this class of complex and multi-step solid-surface chemical reactions.

Acknowledgement

This work was supported by JSPS KAKEMHI Grant Numbers JP21K14723 and JP25K08562 to T.I. The calculations were partly carried out at the Academic Center for Computing and Media Studies (ACCMS) at Kyoto University and at Research Center for Computational Science, Okazaki, Japan (Projects: 23-IMS-C058, 24-IMS-C057, and 25-IMS-C058).

Supporting Information Available

Details of potential-scaling molecular dynamics simulations for structure generation, density functional based tight-binding and density functional theory calculations for structure refinement, calculation system and conditions, nudged elastic band calculations for Mg^{2+} dissolution, and potential-scaling molecular dynamics simulations for nucleation in water; Potential energy variation of interfacial structures; and Supplementary tables and figures noted in the main text. Parameter file for reactive force field (ReaxFF) calculations (ffield.txt). This material is available free of charge via the Internet at <http://pubs.acs.org/>.

References

- (1) Giauque, W. F.; Archibald, R. C. The Entropy of Water from the Third Law of Thermodynamics. The Dissociation Pressure and Calorimetric Heat of the Reaction $\text{Mg(OH)}_2 = \text{MgO} + \text{H}_2\text{O}$. The Heat Capacities of Mg(OH)_2 and MgO from 20 to 300°K. *J. Am. Chem. Soc.* **1937**, *59*, 561–569.
- (2) Chen, L.-Q. Phase-Field Models for Microstructure Evolution. *Annu. Rev. Mater. Res.* **2002**, *32*, 113–140.
- (3) Chang, Y.; Chen, S.; Zhang, F.; Yan, X.; Xie, F.; Schmid-Fetzer, R.; Oates, W. Phase diagram calculation: past, present and future. *Prog. Mater. Sci.* **2004**, *49*, 313–345.
- (4) Björneholm, O.; Hansen, M. H.; Hodgson, A.; Liu, L.-M.; Limmer, D. T.; Michaelides, A.; Pedevilla, P.; Rossmeisl, J.; Shen, H.; Tocci, G.; Tyrode, E.; Walz, M.-M.; Werner, J.; Bluhm, H. Water at Interfaces. *Chem. Rev.* **2016**, *116*, 7698–7726.
- (5) Yan, T.; Wang, R.; Li, T.; Wang, L.; Fred, I. T. A review of promising candidate reactions for chemical heat storage. *Renew. Sustain. Energy Rev.* **2015**, *43*, 13–31.
- (6) Carrillo, A. J.; González-Aguilar, J.; Romero, M.; Coronado, J. M. Solar Energy on Demand: A Review on High Temperature Thermochemical Heat Storage Systems and Materials. *Chem. Rev.* **2019**, *119*, 4777–4816.
- (7) Kato, Y.; Yamashita, N.; Kobayashi, K.; Yoshizawa, Y. Kinetic study of the hydration of magnesium oxide for a chemical heat pump. *Appl. Therm. Eng.* **1996**, *16*, 853–862.
- (8) Hewlett, P. C. *Lea's Chemistry of Cement and Concrete*, 4th ed.; Arnold: London, 1998.
- (9) Dung, N.; Unluer, C. Development of MgO concrete with enhanced hydration and carbonation mechanisms. *Cem. Concr. Res.* **2018**, *103*, 160–169.
- (10) Ma, S.; Akca, A. H.; Esposito, D.; Kawashima, S. Influence of aqueous carbonate species on hydration and carbonation of reactive MgO cement. *J. CO2 Util.* **2020**, *41*, 101260.

(11) Cadigan, C. A.; Corpuz, A. R.; Lin, F.; Caskey, C. M.; Finch, K. B. H.; Wang, X.; Richards, R. M. Nanoscale (111) faceted rock-salt metal oxides in catalysis. *Catal. Sci. Technol.* **2013**, *3*, 900–911.

(12) Di Cosimo, J. I.; Díez, V. K.; Ferretti, C.; Apesteguía, C. R. In *Catalysis*; Spivey, J. J., Han, Y.-F., Dooley, K. M., Eds.; Royal Society of Chemistry: Cambridge, UK, 2014; Vol. 26; pp 1–28.

(13) Kondo, A.; Kurosawa, R.; Ryu, J.; Matsuoka, M.; Takeuchi, M. Investigation on the Mechanisms of Mg(OH)₂ Dehydration and MgO Hydration by Near-Infrared Spectroscopy. *J. Phys. Chem. C* **2021**, *125*, 10937–10947.

(14) Pettauer, M.; Baldermann, A.; Eder, S.; Dietzel, M. Hydration of MgO: Reaction Kinetics and pH Control on Brucite Crystal Morphology. *Cryst. Growth Des.* **2024**, *24*, 3085–3092.

(15) Wu, M.; Estrada, C. A.; Corneille, J. S.; Goodman, D. W. Model surface studies of metal oxides: Adsorption of water and methanol on ultrathin MgO films on Mo(100). *J. Chem. Phys.* **1992**, *96*, 3892–3900.

(16) Xu, C.; Goodman, D. Structure and geometry of water adsorbed on the MgO(100) surface. *Chem. Phys. Lett.* **1997**, *265*, 341–346.

(17) Liu, P.; Kendelewicz, T.; Brown, G. E.; Parks, G. A. Reaction of water with MgO(100) surfaces. Part I: Synchrotron X-ray photoemission studies of low-defect surfaces. *Surf. Sci.* **1998**, *412-413*, 287–314.

(18) Ferry, D.; Picaud, S.; Hoang, P.; Girardet, C.; Giordano, L.; Demirdjian, B.; Suzanne, J. Water monolayers on MgO(100): structural investigations by LEED experiments, tensor LEED dynamical analysis and potential calculations. *Surf. Sci.* **1998**, *409*, 101–116.

(19) Finocchi, F.; Hacquart, R.; Naud, C.; Jupille, J. Hydroxyl-defect Complexes on Hydrated MgO Smokes. *J. Phys. Chem. C* **2008**, *112*, 13226–13231.

(20) Giordano, L.; Goniakowski, J.; Suzanne, J. Partial Dissociation of Water Molecules in the (3×2) Water Monolayer Deposited on the MgO (100) Surface. *Phys. Rev. Lett.* **1998**, *81*, 1271–1273.

(21) Odelius, M. Mixed Molecular and Dissociative Water Adsorption on MgO[100]. *Phys. Rev. Lett.* **1999**, *82*, 3919–3922.

(22) Delle Site, L.; Alavi, A.; Lynden-Bell, R. M. The structure and spectroscopy of monolayers of water on MgO: An ab initio study. *J. Chem. Phys.* **2000**, *113*, 3344–3350.

(23) Jug, K.; Heidberg, B.; Bredow, T. Cyclic cluster study of water adsorption structures on the MgO(100) surface. *Surf. Sci.* **2007**, *601*, 1529–1535.

(24) Włodarczyk, R.; Sierka, M.; Kwapień, K.; Sauer, J.; Carrasco, E.; Aumer, A.; Gomes, J. F.; Sterrer, M.; Freund, H.-J. Structures of the Ordered Water Monolayer on MgO(001). *J. Phys. Chem. C* **2011**, *115*, 6764–6774.

(25) Sassi, M.; Rosso, K. M. First principles simulations of MgO(100) surface hydration at ambient conditions. *Phys. Chem. Chem. Phys.* **2024**, *26*, 2269–2276.

(26) Adhikari, N. M.; Tuladhar, A.; Wang, Z.; De Yoreo, J. J.; Rosso, K. M. No Hydrogen Bonding between Water and Hydrophilic Single Crystal MgO Surfaces? *J. Phys. Chem. C* **2021**, *125*, 26132–26138.

(27) Ončák, M.; Włodarczyk, R.; Sauer, J. Hydration Structures of MgO, CaO, and SrO (001) Surfaces. *J. Phys. Chem. C* **2016**, *120*, 24762–24769.

(28) Mejias, J. A.; Berry, A. J.; Refson, K.; Fraser, D. G. The kinetics and mechanism of MgO dissolution. *Chem. Phys. Lett.* **1999**, *314*, 558–563.

(29) Jug, K.; Heidberg, B.; Bredow, T. Molecular Dynamics Study of Water Adsorption Structures on the MgO(100) Surface. *J. Phys. Chem. C* **2007**, *111*, 6846–6851.

(30) Jug, K.; Heidberg, B.; Bredow, T. Cyclic Cluster Study on the Formation of Brucite from Periclase and Water. *J. Phys. Chem. C* **2007**, *111*, 13103–13108.

(31) Ončák, M.; Włodarczyk, R.; Sauer, J. Water on the MgO(001) Surface: Surface Reconstruction and Ion Solvation. *J. Phys. Chem. Lett.* **2015**, *6*, 2310–2314.

(32) Ishida, T.; Ishimura, K. Chemical Heat Storage Mechanism in Alkaline Earth Metal Oxide: Ab Initio Modeling of the Initial Hydration Reaction on MgO(001) Surface. *J. Phys. Chem. C* **2024**, *128*, 7397–7407.

(33) Carrasco, E.; Brown, M. A.; Sterrer, M.; Freund, H.-J.; Kwapien, K.; Sierka, M.; Sauer, J. Thickness-Dependent Hydroxylation of MgO(001) Thin Films. *J. Phys. Chem. C* **2010**, *114*, 18207–18214.

(34) Wogelius, R. A.; Refson, K.; Fraser, D. G.; Grime, G. W.; Goff, J. P. Periclase surface hydroxylation during dissolution. *Geochim. Cosmochim. Acta* **1995**, *59*, 1875–1881.

(35) Oviedo, J.; Calzado, C. J.; Sanz, J. F. Molecular dynamics simulations of the MgO(001) surface hydroxylation. *J. Chem. Phys.* **1998**, *108*, 4219–4225.

(36) Lee, J.; Eun, J.; Kim, S.; Park, S.; Lee, M.; Kim, H. Hydration behavior of MgO single crystals and thin films. *J. Mater. Res.* **2003**, *18*, 2895–2903.

(37) Rocha, S. D.; Mansur, M. B.; Ciminelli, V. S. Kinetics and mechanistic analysis of caustic magnesia hydration. *J. Chem. Tech. Biotechnol.* **2004**, *79*, 816–821.

(38) Sasahara, A.; Murakami, T.; Tomitori, M. Hydration of MgO(100) Surface Promoted at $\langle 011 \rangle$ Steps. *J. Phys. Chem. C* **2015**, *119*, 8250–8257.

(39) Kuleci, H.; Schmidt, C.; Rybacki, E.; Petrishcheva, E.; Abart, R. Hydration of periclase at 350 °C to 620 °C and 200 MPa: experimental calibration of reaction rate. *Miner. Petrol.* **2016**, *110*, 1–10.

(40) Amaral, L.; Oliveira, I.; Salomão, R.; Frollini, E.; Pandolfelli, V. Temperature and common-ion effect on magnesium oxide (MgO) hydration. *Ceram. Int.* **2010**, *36*, 1047–1054.

(41) Chen, M.; Dixon, D. A. Structure and Stability of Hydrolysis Reaction Products of MgO Nanoparticles Leading to the Formation of Brucite. *J. Phys. Chem. C* **2017**, *121*, 21750–21762.

(42) Tang, X.; Nie, Y.; Jin, Q.; Guo, L.; Zhao, J.; Li, T.; Zhu, Y. Kinetics and mechanism of ultrasonic-assisted magnesium oxide hydration. *Ultrason. Sonochem.* **2018**, *40*, 995–1002.

(43) Maltseva, A.; Shkirskiy, V.; Lefèvre, G.; Volovitch, P. Effect of pH on Mg(OH)₂ film evolution on corroding Mg by in situ kinetic Raman mapping (KRM). *Corros. Sci.* **2019**, *153*, 272–282.

(44) Bracco, J. N.; Camacho Meneses, G.; Colón, O.; Yuan, K.; Stubbs, J. E.; Eng, P. J.; Wanhal, A. K.; Einkauf, J. D.; Boebinger, M. G.; Stack, A. G.; Weber, J. Reaction Layer Formation on MgO in the Presence of Humidity. *ACS Appl. Mater. Interfaces* **2024**, *16*, 712–722.

(45) Feitknecht, W.; Braun, H. Der Mechanismus der Hydratation von Magnesiumoxid mit Wasserdampf. *Helv. Chim. Acta* **1967**, *50*, 2040–2053.

(46) Refson, K.; Wogelius, R. A.; Fraser, D. G.; Payne, M. C.; Lee, M. H.; Milman, V. Water chemisorption and reconstruction of the MgO surface. *Phys. Rev. B* **1995**, *52*, 10823–10826.

(47) Asaduzzaman, A. The hydration of periclase: Atomistic insights from quantum-chemical look. *Chem. Phys.* **2020**, *532*, 110694.

(48) Vermilyea, D. A.; Kirk, C. F. Studies of Inhibition of Magnesium Corrosion. *J. Electrochem. Soc.* **1969**, *116*, 1487.

(49) Baumann, S. O.; Schneider, J.; Sternig, A.; Thomele, D.; Stankic, S.; Berger, T.; Grönbeck, H.; Diwald, O. Size Effects in MgO Cube Dissolution. *Langmuir* **2015**, *31*, 2770–2776.

(50) Luong, N. T.; Holmboe, M.; Boily, J.-F. MgO nanocube hydroxylation by nanometric water films. *Nanoscale* **2023**, *15*, 10286–10294.

(51) Luong, N. T.; Boily, J.-F. Water Film-Driven Brucite Nanosheet Growth and Stacking. *Langmuir* **2023**, *39*, 11090–11098.

(52) Ewing, G. E. Ambient Thin Film Water on Insulator Surfaces. *Chem. Rev.* **2006**, *106*, 1511–1526.

(53) Inagaki, T.; Saito, S. Hybrid Monte Carlo method with potential scaling for sampling from the canonical multimodal distribution and imitating the relaxation process. *J. Chem. Phys.* **2022**, *156*, 104111.

(54) van Duin, A. C. T.; Dasgupta, S.; Lorant, F.; Goddard, W. A. ReaxFF: A Reactive Force Field for Hydrocarbons. *J. Phys. Chem. A* **2001**, *105*, 9396–9409.

(55) Elstner, M.; Porezag, D.; Jungnickel, G.; Elsner, J.; Haugk, M.; Frauenheim, T.; Suhai, S.; Seifert, G. Self-consistent-charge density-functional tight-binding method for simulations of complex materials properties. *Phys. Rev. B* **1998**, *58*, 7260–7268.

(56) Sprik, M.; Hutter, J.; Parrinello, M. Ab initio molecular dynamics simulation of liquid water: Comparison of three gradient-corrected density functionals. *J. Chem. Phys.* **1996**, *105*, 1142–1152.

(57) Hazen, R. M. Effects of temperature and pressure on the cell dimension and X-ray temperature factors of periclase. *Am. Mineral.* **1976**, *61*, 266–271.

(58) Laporte, S.; Finocchi, F.; Paulatto, L.; Blanchard, M.; Balan, E.; Guyot, F.; Saitta, A. M. Strong electric fields at a prototypical oxide/water interface probed by ab initio molecular dynamics: MgO(001). *Phys. Chem. Chem. Phys.* **2015**, *17*, 20382–20390.

(59) Ding, Z.; Selloni, A. Hydration structure of flat and stepped MgO surfaces. *J. Chem. Phys.* **2021**, *154*, 114708.

(60) Luzar, A.; Chandler, D. Effect of Environment on Hydrogen Bond Dynamics in Liquid Water. *Phys. Rev. Lett.* **1996**, *76*, 928–931.

(61) Choudhary, A.; Chandra, A. Anisotropic structure and dynamics of the solvation shell of a benzene solute in liquid water from ab initio molecular dynamics simulations. *Phys. Chem. Chem. Phys.* **2016**, *18*, 6132–6145.

(62) Kim, S.; Wang, X.; Jang, J.; Eom, K.; Clegg, S. L.; Park, G.-S.; Di Tommaso, D. Hydrogen-Bond Structure and Low-Frequency Dynamics of Electrolyte Solutions: Hydration Numbers from ab Initio Water Reorientation Dynamics and Dielectric Relaxation Spectroscopy. *ChemPhysChem* **2020**, *21*, 2334–2346.

(63) McCarthy, M. I.; Schenter, G. K.; Scamehorn, C. A.; Nicholas, J. B. Structure and Dynamics of the Water/MgO Interface. *J. Phys. Chem.* **1996**, *100*, 16989–16995.

(64) Zimmermann, N. E. R.; Vorselaars, B.; Quigley, D.; Peters, B. Nucleation of NaCl from Aqueous Solution: Critical Sizes, Ion-Attachment Kinetics, and Rates. *J. Am. Chem. Soc.* **2015**, *137*, 13352–13361.

(65) Smithson, G. L.; Bakhshi, N. N. The kinetics and mechanism of the hydration of magnesium oxide in a batch reactor. *Can. J. Chem. Eng.* **1969**, *47*, 508–513.

(66) Thomas, J. J.; Musso, S.; Prestini, I. Kinetics and Activation Energy of Magnesium Oxide Hydration. *J. Am. Ceram. Soc.* **2014**, *97*, 275–282.

(67) Hu, X. L.; Klimeš, J.; Michaelides, A. Proton transfer in adsorbed water dimers. *Phys. Chem. Chem. Phys.* **2010**, *12*, 3953–3956.

(68) Rimsza, J. M.; Sorte, E. G.; Alam, T. M. Hydration and Hydroxylation of MgO in Solution: NMR Identification of Proton-Containing Intermediate Phases. *ACS Omega* **2019**, *4*, 1033–1044.

(69) Xing, Z.; Bai, L.; Ma, Y.; Wang, D.; Li, M. Mechanism of Magnesium Oxide Hydration

Based on the Multi-Rate Model. *Materials* **2018**, *11*.

Table of Contents (TOC) graphics.

